Strong chiral optical response from planar arrays of subwavelength metallic structures supporting surface plasmon resonances

F. Eftekhari and T. J. Davis

CSIRO Materials Science and Engineering, Private Bag 33 Clayton, Victoria 3168, Australia and Melbourne Centre for Nanofabrication 151 Wellington Road Clayton, Victoria 3168, Australia

(Received 25 May 2012; revised manuscript received 24 July 2012; published 13 August 2012)

A strong differential response in the scattering of left and right circularly polarized light from surface plasmons in planar metal nanostructures is investigated theoretically and experimentally. We show that a strong chiral optical response can be obtained by an interference effect arising from a combination of resonance phase shifts in the metal structures and phase shifts associated with the rotation of the electric field vector. The effect is modeled using an analytical theory of localized surface plasmon resonances which predicts a maximum in the chiral response when the nanostructure exhibits at least two resonant modes, separated in frequency by $\Gamma/\sqrt{3}$, where Γ is the FWHM of the resonance, and when the angle between the dipole moments of the modes is oriented at 45 degrees. The predictions of the model agree well with numerical simulations based on the finite-difference time-domain method. The interference effect is demonstrated by optical measurements on planar metamaterials consisting of subwavelength arrays of gold rods. The effect is not related to optical activity, circular dichroism, diffraction, or phase shifts on propagation. The failure to satisfy the conditions for interference explains why some geometrically chiral structures show little or no differential scattering with circularly polarized incident light. This work provides criteria for designing new plasmonic nanostructures with strong chiral optical response.

DOI: 10.1103/PhysRevB.86.075428 PACS number(s): 78.67.Bf, 42.25.Ja, 73.20.Mf, 78.20.Bh

I. INTRODUCTION

Chiral symmetry refers to a certain handedness in geometry such that a chiral object and its mirror image cannot be rotated or translated to align perfectly. Light itself can be chiral and a measure of optical chirality was recently introduced[1,2] that changes sign from left circular polarization (LCP) to right circular polarization (RCP). There has been interest in using localized surface plasmon resonances in metallic nanostructures to create nanoscale thin films with a high sensitivity to the chirality of light.[3–14] In many cases, the thin films consist of subwavelength arrays of structures that are nondiffracting. In this regard the subwavelength unit acts as a *meta-atom* and the thin film is described as a *metamaterial*.

The geometric requirements of nanostructures to exhibit a strong response to optical chirality are not well understood. The structures shown in Figs. 1(a)–1(c) have obvious geometric chirality but, when arrayed on a surface, exhibit little or no chiral optical response.[5–7,9,10] However, the structures in Figs. 1(d)–1(f) have less obvious chirality but demonstrate a range of responses, some of them large.[3,4,8,13,14] The question arises as to what features are required of the meta-atom to scatter light with RCP differently from LCP. It has been discussed that true optical activity (OA) or circular dichroism (CD) requires certain symmetry properties that are not satisfied with thin planar structures.[15] Furthermore, OA and CD are usually associated with magnetic dipole interactions. Here we propose a mechanism for achieving a strong chiral optical response from thin metal nanostructures that exploits an asymmetry in the phase shifts between localized surface plasmon (LSP) resonances. This mechanism leads to interference between the light scattered from the LSPs resulting in constructive or destructive interference in the far field that depends on the chirality of the incident light. The effect is purely electrical in nature and is not related to OA or CD and can arise in subwavelength planar structures. The interference arises from phase shifts at the subwavelength scale and differs from diffraction associated with periodic structures and from interference effects arising from phase shifts on propagation.

In Sec. II we begin with a qualitative discussion of how the phases of LSP resonances can be manipulated to scatter light depending on the state of circular polarization. We show that two phase shift mechanisms combine in an asymmetrical fashion to create chiral-sensitive scattering. An approximate analytical model of surface plasmon resonances is used to derive the conditions necessary to maximize the chiral optical response. The conditions relate the interference effect to the phase shifts associated with the LSP resonances and to the orientations of their dipole moments. In Sec. III we describe the numerical solutions to the full Maxwell equations applied to an example system consisting of two gold nanorods. The simulations show excellent agreement with the analytical model. Demonstrations of the interference effect based on optical experiments on metamaterials are also presented. A discussion of the results and their implication in terms of previous experiments on metal nanostructures is given in Sec. IV.

II. THEORY

In this section we examine the interaction of circularly polarized light with an arbitrary collection of interacting metal nanostructures supporting LSP resonances. We begin with a qualitative discussion of how a metal nanostructure can be configured to scatter light depending on its chirality and then we use an analytical model of LSP resonances to quantify the effect.

A. Far-field interference arising from LSP resonances

Surface plasmons are charge oscillations excited by light on the surface of a metal. At a particular excitation frequency, the charge oscillation forms a standing wave over the metal

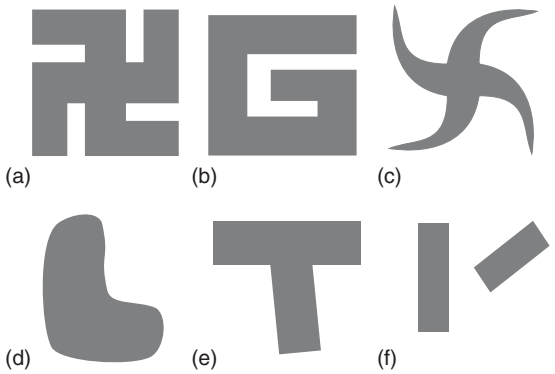

FIG. 1. Examples of planar plasmonic nanostructures that exhibit geometric chirality but varying degrees of optical chirality: (a)–(c) these structures have been shown to have no chiral optical response; (d)–(f) these structures are not obviously chiral but show quite strong differential response to left and right circularly polarized light.

surface, which is described as a localized surface plasmon resonance. The distribution of charge depends strongly on the geometry of the nanostructure and can be represented by a large number of multipoles (such as dipoles, quadrupoles, etc.). In the far field, the light scattering depends predominantly on the dipole moment of this distribution, particularly for subwavelength structures resonating at the fundamental mode. This allows us to focus on the dipole moment of this mode with regard to scattering in the far field and the interaction between the incident light and the metal nanostructures.

To understand the interference effect, we consider a metal structure that supports two LSP modes with dipole moments that are not parallel. An example of such a structure is shown in Fig. 2 where the LSP modes are misaligned by an angle of about $\pi/4$. We consider circularly polarized incident light where the electric field vector rotates in the plane of the metal structure. At one moment the field aligns with the dipole moment of one mode and then, at a later time, aligns with the dipole moment of the other mode. This induces a phase shift between the LSP resonances, shown as the dashed curves in Fig. 2. We refer to this as the *rotation-induced phase shift*. On changing the chirality of the light (that is from LCP to RCP), the direction of rotation of the electric field vector reverses, changing the sign of the phase shift between the modes. In the far field this would produce no effect since the intensity depends only on the magnitude of the phase difference.

However, the LSP resonances themselves may have a phase shift relative to the incident light that is determined by their resonance frequency. This phase shift is small when the frequency of the incident light is well below the LSP resonance frequency; it passes through $\pi/2$ as the frequencies coincide and then approaches π as the incident frequency becomes large. Importantly, the resonance phases are independent of the chirality of the light. The resonance phase shift and the rotation-induced phase shift combine to determine the final phase of each LSP resonance. The oscillations that include both phase shift effects are shown by the solid lines in Fig. 2. The phase difference $\Delta\phi$ between these two oscillations controls the degree of interference and changes with the chirality of the incident light. By a suitable orientation of LSP dipole moments and an appropriate adjustment of their

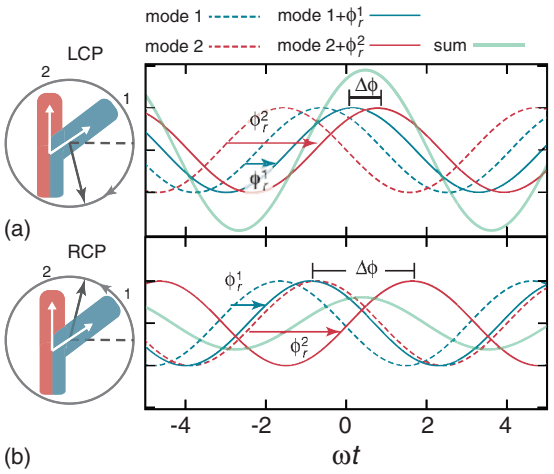

FIG. 2. (Color online) Diagrams showing the oscillations of two LSP modes relative to the incident field for (a) LCP and (b) RCP. The colors represent the two different LSP modes and the white arrows on the structures indicate the orientations of the LSP dipole moments. The dashed curves in the graphs show the LSP oscillations with time, in units of ωt, excluding the resonance phase shifts. The relative phases of the oscillations change sign with incident light changing from LCP to RCP. The solid lines include the phase differences due to the resonances (mode 1: $\phi_r^1 = \pi/4$; mode 2: $\phi_r^2 = 3\pi/4$). The combined phase difference $\Delta\phi$ determines the amplitude of the sum of the oscillations that affects the intensity in the far field.

resonance frequencies, the light scattered into the far field from two LSP modes can interfere constructively or destructively, depending on the chirality of the light.

B. Analytical model

To quantify the interference effect, we use an analytical model for an arbitrary collection of interacting plasmonic nanostructures. This model has been used previously to study different plasmonic systems.[16–20] The response to the incident light field is modeled in terms of sums over the optically resonant modes—these are the LSP resonances[16] excited by an incident light field $\mathbf{E}_0 \exp(-i\omega t)$. The model uses an eigenmode expansion for the self-consistent surface charge distribution, based on the electrostatic approximation, and is applicable to systems much smaller than the wavelength of light (Rayleigh limit). In this limit we ignore the phase delays due to wave propagation, which decouples the electric and magnetic fields. Even with this approximation, the model is capable of describing complex LSP resonances involving high-order multipoles[21] as well as the resonance shifts arising from coupling between the LSP modes in ensembles of metal nanostructures.[16,18,20] We emphasise that the excitation of a complex LSP resonance by an incident plane wave is predominantly through the dipole moment of the resonance, and the subsequent scattering of light is also determined by the dipole moment.

The strength of the LSP excitation is described by an amplitude $a_r^k(\omega)$ where the subscript r references the different nanostructures and the superscript k references the different

LSP resonances. The excitation amplitude can be written as[18]

$$a_r^k(\omega) = f_r^k(\omega)\mathbf{p}_r^k \cdot \mathbf{E}_0 \approx -\frac{A_r^k \mathbf{p}_r^k \cdot \mathbf{E}_0}{\omega - \omega_r^k + i\Gamma_r^k/2}, \qquad (1)$$

where $\mathbf{E}_0$ is constant over the surface of the nanostructure. The vector $\mathbf{p}_r^k$ is proportional to the dipole moment of the resonant mode[17] and differs from the true dipole moment $\mathbf{p}$ by a scale factor. The resonance factor $f_r^k(\omega)$ is related to the polarizability per unit volume of the structure. This factor is approximated by a term involving the resonance frequency ω_r^k of the mode and a loss term Γ_r^k that arises from a Drude model of the metal permittivity.[18] It is useful to show the phase ϕ_r^k of the resonance explicitly: $f_r^k = |f_r^k| \exp(i\phi_r^k)$.

Note that Eq. (1) is applicable to metallic nanostructures of any complexity, such as one that is composed of a number of separate components. Although the components each have particular LSP resonances, when in close proximity there is an interaction between them mediated by the electric fields from the surface charges. The interaction alters both the resonant modes of the ensemble and the distributions of surface charges.[16] This is often referred to as *hybridization* of the LSP modes.[22] However, the hybridized modes also have well defined resonances[23] that, again, can be represented by excitation amplitudes of the form in Eq. (1). In this regard the meta-atom may consist of a number of separate subwavelength metal structures that interact with one another. We shall exploit this property to demonstrate the dependence of the chiral optical response on the LSP resonances.

At the subwavelength scale the interaction of a metal nanostructure with light is dominated by the dipole moment of the LSP resonance. The time-averaged power per solid angle radiated in the far-field direction $\hat{n}$ by a scatterer with dipole moment $\mathbf{p}$ can be written in the form

$$\frac{dP}{d\Omega} = \frac{ck^4}{32\pi^2\epsilon_0}(\hat{n} \times \mathbf{p}) \cdot (\hat{n} \times \mathbf{p}^*), \qquad (2)$$

where c is the speed of light in vacuum, k is the wave number of the radiation, and ϵ_0 is the permittivity of space.[24] Here $\mathbf{p}^*$ is the complex conjugate of $\mathbf{p}$; the dipole moment is a complex quantity because its oscillations with time are shifted in phase relative to the incident light.

To understand how the plasmonic nanostructure responds to circularly polarized light, we locate the structure on the x-y plane [Fig. 3(a)]. With circularly polarized light incident from above, propagating in the $-\hat{z}$ direction, the electric field vector is uniform over the x-y plane and rotates in time according to $\mathbf{E}(t) = E_0(\hat{x}\cos\omega t \pm \hat{y}\sin\omega t)$. The $\pm$ sign determines whether the light has LCP ($-$) or RCP ($+$). This can be represented in the usual way with complex numbers, $\mathbf{E}_0 = E_0(\hat{x} \pm i\hat{y})$. Using a standard vector identity, the term in Eq. (2) involving the dipole moments can be written as $(\hat{n} \times \mathbf{p}) \cdot (\hat{n} \times \mathbf{p}^*) = \mathbf{p} \cdot \mathbf{p}^* - (\hat{n} \cdot \mathbf{p})(\hat{n} \cdot \mathbf{p}^*)$. The dipole moment of the nanostructure is given by a sum over the dipole moments of the individual LSP modes $\mathbf{p} = \sum_k a_r^k(\omega)\mathbf{p}_r^k$. We write the dipole moment of mode k as $\mathbf{p}_r^k = p_z^k\hat{z} + p_{xy}^k(\cos\theta_r^k\hat{x} + \sin\theta_r^k\hat{y})$ with a projection p_{xy}^k in the x-y plane oriented with angle θ_r^k [see Fig. 3(b)]. The unit vector in the direction of observation can be resolved into components $\hat{n} = \cos\xi\hat{z} + \sin\xi(\cos\psi\hat{x} + \sin\psi\hat{y})$ so that

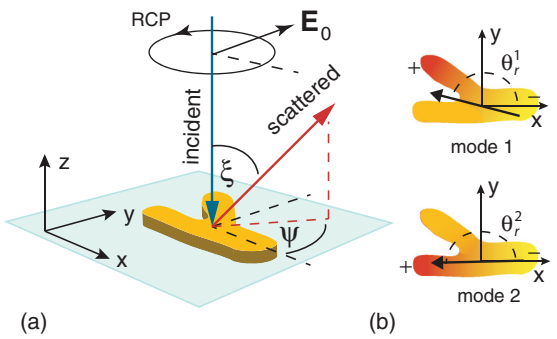

FIG. 3. (Color online) The geometry used in the analytical model. (a) The metal structure on the x-y plane showing the circularly polarized incident light and the direction of the scattered light. (b) A representation of two LSP modes on a single metal nanostructure showing the directions of the dipole moments. The color indicates the relative surface charge of each mode. Note that the LSP dipole moments may not be parallel to the structural features.

$\hat{n} \cdot \mathbf{p}_r^k = \cos\xi p_z^k + \sin\xi\cos(\theta_r^k - \psi)p_{xy}^k$. When placed into Eq. (2), the terms involving the vector cross products take the form $(\hat{n} \times \mathbf{p}_r^k) \cdot (\hat{n} \times \mathbf{p}_r^j) = p_{xy}^k p_{xy}^j(\cos(\theta_r^k - \theta_r^j) + 2N_r^{kj})$ where N_r^{kj} accounts for off-axis scattering. This is defined by

$$\begin{aligned} &2N_r^{kj} p_{xy}^k p_{xy}^j \\ &= p_z^k p_z^j \sin^2\xi - p_{xy}^k p_{xy}^j \sin^2\xi \cos\left(\theta_r^k - \psi\right)\cos\left(\theta_r^j - \psi\right) \\ &\quad -\tfrac{1}{2}\sin 2\xi\left(p_{xy}^k p_z^j \cos\left(\theta_r^k - \psi\right) + p_{xy}^j p_z^k \cos\left(\theta_r^j - \psi\right)\right). \end{aligned} \qquad (3)$$

For scattering normal to the x-y plane, $\xi = 0$ so that $N_r^{kj} = 0$. With circular polarization, the excitation amplitude (1) involves the term $\mathbf{p}_r^k \cdot \mathbf{E}_0 = p_{xy}^k E_0 \exp(\pm i\theta_r^k)$. Since the dipole moment $\mathbf{p}$ is given by a sum over the resonant modes, then Eq. (2) will contain products of sums involving the excitation amplitudes of the form $a_r^k a_r^{j*} = p_{xy}^k p_{xy}^j E_0^2 |f_r^k||f_r^j| \exp[i(\phi_r^k - \phi_r^j) \pm i(\theta_r^k - \theta_r^j)]$. By including pairs of terms in the sum with k and j interchanged, we can write the scattered power in the form

$$\begin{aligned} \frac{dP}{d\Omega} = \frac{ck^4 E_0^2}{32\pi^2\epsilon_0}\sum_k\sum_{j\leqslant k}\left(p_{xy}^k p_{xy}^j\right)^2 |f_r^k||f_r^j|\{&\cos\left(\phi_r^k - \phi_r^j\right) \\ &\times\left[1 + \cos 2\left(\theta_r^k - \theta_r^j\right) + N_r^{kj}\cos\left(\theta_r^k - \theta_r^j\right)\right] \\ &\mp \sin\left(\phi_r^k - \phi_r^j\right)\left[\sin 2\left(\theta_r^k - \theta_r^j\right) + N_r^{kj}\sin\left(\theta_r^k - \theta_r^j\right)\right]\}. \end{aligned} \qquad (4)$$

The last term in this expression depends on the sign of the circular polarization and therefore is the key factor that controls whether or not the scattering is sensitive to the chirality of the incident light. It depends on the phase differences $\phi_r^k - \phi_r^j$ between pairs of resonant LSP modes k and j and it depends on the angle $\theta_r^k - \theta_r^j$ between the projections of the dipole moments of the modes in the x-y plane (this is the plane perpendicular to the direction of propagation of the incident light).

C. Factors affecting chiral optical response

From our analysis above, there are two main factors that affect the response of the nanostructure to the chirality of the incident light. We first consider the effect of the phase differences between the LSP modes.

It is clear from Eq. (4) that a nanostructure with a single resonant mode will not distinguish between LCP and RCP, irrespective of its shape, since $\sin(\phi_r^k - \phi_r^k) = 0$. This statement is based on our derivation within the electrostatic approximation and may be invalid if retardation (propagation phase delay) or magnetic effects are important. In addition the resonant modes cannot have the same frequency—that is, the modes cannot be degenerate—otherwise the phase difference between them is again zero.

The maximum response to optical chirality occurs when $|f_r^k||f_r^j|\sin(\phi_r^k - \phi_r^j)$ is a maximum. From the definition of f_r^k in Eq. (1) we can write

$$\left|f_r^k\right|\left|f_r^j\right|\sin\left(\phi_r^k - \phi_r^j\right) \approx \frac{A_r^k A_r^j\left[\Gamma_r^j\left(\omega - \omega_r^k\right) - \Gamma_r^k\left(\omega - \omega_r^j\right)\right]}{2\left[\left(\omega - \omega_r^j\right)^2 + \Gamma_r^{j2}/4\right]\left[\left(\omega - \omega_r^k\right)^2 + \Gamma_r^{k2}/4\right]}. \quad (5)$$

The applied frequency that maximizes Eq. (5) is found by taking a derivative with respect to ω, setting the resulting expression to zero, and then solving for ω. This leads to a complicated equation. A more useful result is obtained with the further approximation $\Gamma_r^k \approx \Gamma_r^j = \Gamma$. Then it is straightforward to show there are three solutions for the applied frequency that lead to extrema in the differential response. A local minimum occurs at frequency $\omega = \omega_{\text{av}}^{kj}$ and two maxima occur at $\omega = \omega_{\text{av}}^{kj} \pm [(\omega_{\text{dif}}^{kj})^2 - \Gamma^2]^{1/2}/2$. In this expression $\omega_{\text{av}}^{kj} = (\omega_r^k + \omega_r^j)/2$ is the average of the two resonances and $\omega_{\text{dif}}^{kj} = \omega_r^k - \omega_r^j$ is the difference. The two maxima merge with the minimum when $|\omega_{\text{dif}}^{kj}| < \Gamma$ where the term in the square root becomes negative. When this occurs, the optimum applied frequency is at $\omega = \omega_{\text{av}}^{kj}$ which is the average of the two resonances. When this optimum frequency is placed into Eq. (5) and the derivative taken with respect to ω_{dif}^{kj}, we find that the maximum optical chiral response occurs where the two resonances are separated by $|\omega_{\text{dif}}^{kj}| = \Gamma/\sqrt{3}$. The loss term Γ is the full width at half maximum of each resonance. In Fig. 4(a) we have evaluated $|f_r^k||f_r^j|\sin(\phi_r^k - \phi_r^j)$ as a function of frequency for different resonance separations. This shows the two maxima and the minimum which merge and form a single peak, for the conditions as predicted.

The differential response to LCP and RCP also depends on the relative orientation $\theta_r^k - \theta_r^j$ of the dipole moments of the modes. With the observation direction normal to the plane of the polarization, $N_r^{kj} = 0$, the structure will be sensitive to the chirality of the light when $\sin 2(\theta_r^k - \theta_r^j) \neq 0$, implying that the dipole moments of the modes cannot be parallel or perpendicular. Our theory predicts a maximum differential response occurs when $\theta_r^k - \theta_r^j = \pi/4$. This is a trade-off between maximizing the rotation-induced phase difference between the modes, which would occur at $\pi/2$, and maximizing the interference between the scattered light, which occurs when the electric field vectors are parallel and therefore requires the LSP modes to be parallel.

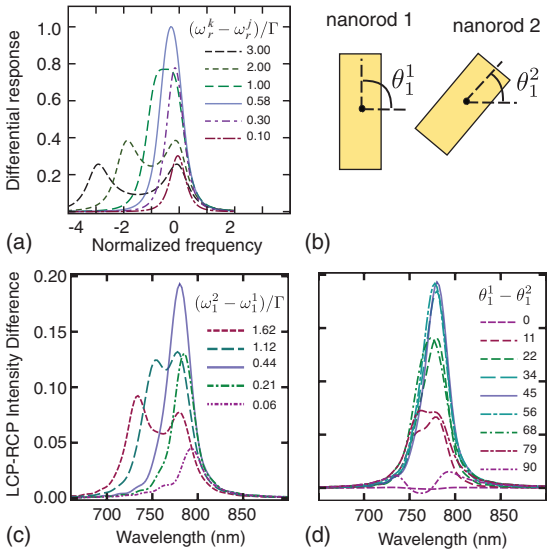

FIG. 4. (Color online) (a) The term $|f_r^k||f_r^j|\sin(\phi_r^k - \phi_r^j)$ as a function of normalized frequency $(\omega - \omega_r^k)/\Gamma$ for a range of resonance differences $(\omega_r^k - \omega_r^j)/\Gamma$. The optimum frequency difference (solid line) occurs for $(\omega_r^k - \omega_r^j)/\Gamma = 1/\sqrt{3} \approx 0.58$. (b) The two nanorods used in the FDTD simulation, representing a single meta-atom. Both nanorods are 25 nm wide, 20 nm thick, and made from gold embedded in a medium with permittivity $\epsilon = 2$. Nanorod 1 is 75 nm long with an orientation fixed at $\theta_1^1 = 90°$ and the length of nanorod 2 was varied. (c) The scattering intensity difference calculated using FDTD for different resonances of nanorod 2 with $\theta_1^2 = 45°$. The resonances were altered by changing its length: 60, 65, 66.5, 68, and 70 nm. (d) The calculated dependence of the scattering intensity difference on θ_1^2 with nanorod 2, $l_2 = 66.5$ nm.

III. EXPERIMENTS

As shown above, we have reduced the problem of creating a structure with a strong chiral optical response to two simple criteria involving the orientation of the dipole moments of the LSP modes and the phase differences between their oscillations. These relationships apply irrespective of the shape or complexity of the metal nanostructures. However, for the analysis to be valid the structures must be smaller than the wavelength of light and must not involve magnetic effects. Since the analytical model is approximate, in that it is based on an electrostatic condition, we compare the predictions against numerical solutions to the full Maxwell equations using a finite-difference time-domain (FDTD) simulation. We also demonstrate the interference effect with optical measurements on metamaterials consisting of arrays of gold rods fabricated on a glass substrate.

A. Numerical simulation

In this simulation the meta-atom consists of a pair of gold nanorods, shown in Fig. 4(b) with each rod exhibiting a single LSP resonance in the wavelength range of interest. This configuration has been proposed by Chigrin *et al.*[13,14] If the interaction between the LSPs is small, the LSP resonance on

each rod will represent a resonant mode of the meta-atom and the mode frequencies will depend on the length of each rod. Furthermore the mode dipole moment will be approximately parallel to the resonating rod; the dipole direction changes with the rod orientation.

Using the FDTD method, we calculated the difference in the scattered intensities for LCP and RCP to measure the differential response, corresponding to the last term in Eq. (4). A Lorentz model of permittivity was used for the gold where the model parameters were adjusted to give good fits to experimental permittivity data in the wavelength range 500 nm to 3 microns. The results of the calculations of the transmitted intensity associated with a single meta-atom are shown in Figs. 4(c)–4(d). In Fig. 4(c) the nanorod orientation was fixed at 45° but the length of the second rod was increased to change its resonance frequency. The curves show the same double peak as in our analytical model [Fig. 4(a)] which merges near $\omega_1^2 - \omega_1^1 = \Gamma$. The peak of the spectrum reaches a maximum close to the predicted value of $|\omega_{\rm dif}^{12}|/\Gamma = 1/\sqrt{3}$. Figure 4(d) shows the effect of changes in orientation, calculated with $|\omega_{\rm dif}^{12}|/\Gamma = 0.44$. We find the maximum differential response occurs for $\theta_r^1 - \theta_r^2 = 45°$, also in agreement with our analytical model. This differs from the numerical simulations of Chigrin, Zhukovski, and Kremers[13,14] who found that two rods resonating at radio frequencies produced a maximum circular dichroism when $\theta_r^1 - \theta_r^2 = 22.5°$. However, as we discuss below, the effect we are measuring is based on interference and does not involve optical activity or circular dichroism.

B. Optical measurements on planar metamaterials

To demonstrate the interference effects predicted by the model, we performed optical experiments on planar metamaterials consisting of arrays of gold nanorods fabricated on glass, as in Fig. 5(a). The arrays were subwavelength with a periodicity of 250 nm. The optical experiments were carried out on a Nikon Ti-Eclipse inverted microscope using a tungsten filament white light source. The light was collimated and passed through a linear polarizer and a broadband quarter-wave plate to control the polarization state. The light transmitted through the metamaterial was collected with a ×40 lens and analyzed in a spectrometer. The light transmitted through the glass substrate in the absence of the metamaterial was also analysed to provide flat-field calibration data.

As with the FDTD simulation, the length l_2 of the second rod was varied to alter its resonance frequency and arrays of nanorod pairs were fabricated with different angles between them. For comparison, we also fabricated arrays of the individual rods. The extinction $E = 1 - T$ related to the transmittance T is shown in Fig. 5(b) for each of the arrays of individual rods under two orthogonal states of linear polarization. The longitudinal modes of the two sets of rods have resonances at 720 and 660 nm. There is also a transverse resonance at 560 nm due to LSP excitation across the width of each rod.

Measurements of the differential extinction for arrays of nanorod pairs ($l_1 = 100$ nm and $l_2 = 80$ nm) with angles between them varying from 0 to 90 degrees are shown in Fig. 5(c). These data show the increase in chiral optical response as the angle approaches 45 degrees, with a maximum

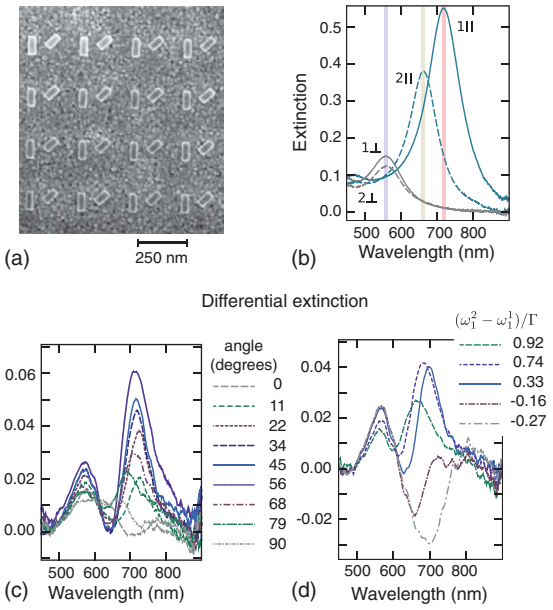

FIG. 5. (Color online) (a) An SEM image of the ebeam resist pattern on a gold film prior to etching. After etching the exposed gold is removed leaving gold nanorods in the same pattern as the resist. (b) The extinction spectra from arrays of single nanorods obtained with linearly polarized light parallel and perpendicular to the long axes of the rods. Nanorod 1 is 100 nm long and nanorod 2 is 80 nm long. Both sets of rods are 30 nm thick and 40 nm wide (c) The difference in the extinction for LCP and RCP for sets of nanorods with rod 2 at different angles. (d) The difference in the extinction for sets of rods with nanorod 2 lengths of 60, 70, 80, 90, and 100 nm. This shifts the resonances so that the relative frequency differences are 0.92, 0.74, 0.33, −0.16, and −0.22 respectively.

occurring at 54 degrees, close to the predictions of our analytical model and the FDTD simulations [compare with Fig. 4(d)]. The chiral optical response associated with the transverse resonances is also seen in this figure.

The experimental results on the arrays with nanorod pairs oriented at 45 degrees, but with the length of nanorod 2 varied from $l_2 = 60$ nm to $l_2 = 100$ nm in steps of 10 nm, are shown in Fig. 5(d). Again, we observe the peak around 700 nm increasing with l_2, reaching a maximum between $l_2 = 70$ nm and $l_2 = 80$ nm [close to $(\omega_1^2 - \omega_1^1)/\Gamma = 1/\sqrt{3}$] and then decreasing again. This behavior is predicted by the analytical model and also appeared in the data from the FDTD simulation. The change in sign of the differential extinction for rod 2 of length close to that of rod 1 is probably due to coupling of the LSP modes as the rod length increases, leading to hybridization of the modes.[18] This changes the orientations of the dipole moments of the modes relative to the orientations of the rods and also alters the mode frequencies. The double peak predicted by the model and the FDTD simulations is not seen in the experiment but may be obscured by the transverse resonance.

To compare the theoretical model with the FDTD numerical simulations (Fig. 4) and the experimental results (Fig. 5), we have extracted data for the differential extinction as functions of angle $\theta_1^1 - \theta_1^2$ [Fig. 6(a)] and as functions of the normalized difference between the resonance frequencies of the modes $(\omega_1^2 - \omega_1^1)/\Gamma$ [Fig. 6(b)]. In Fig. 6(a), the peak

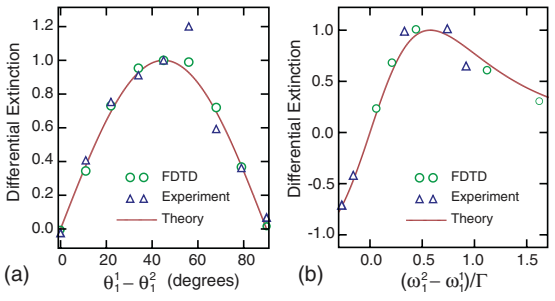

FIG. 6. (Color online) The normalized peak extinction differences associated with left and right circularly polarized light as functions of (a) nanorod angle and (b) resonance difference, as obtained from FDTD numerical simulations (circles), experimental results (triangles), and theory (solid line). The size of the triangles relates to the approximate errors in the measurements.

differential extinction values were normalized against their values at $\theta_1^1 - \theta_1^2 = 45^\circ$ and then plotted against angle. The theoretical prediction obtained from Eq. (4) is $\sin 2(\theta_1^1 - \theta_1^2)$. We observe excellent agreement between theory, simulations, and experiment, apart from the experimental value at 54 degrees that appears as an outlier compared to the rest of the data. The origin of this is unknown.

In Fig. 6(b), the peak differential extinction from the experimental data, and the differential extinction at the average of the two resonances from the FDTD data, are compared with the theoretical model. Again, the data have been normalized, this time to their values closest to $(\omega_1^2 - \omega_1^1)/\Gamma = 1/\sqrt{3}$. The theoretical curve is found from Eq. (5) by setting $\Gamma_1^1 = \Gamma_1^2 = \Gamma$ and the applied frequency to the average of the two resonances $\omega = (\omega_1^1 + \omega_1^2)/2$. This yields a theoretical curve given by $x/(x^2+1)^2$ where $x = (\omega_1^2 - \omega_1^1)/\Gamma$. Again we see excellent agreement between theory, simulations, and experiment. Note that the theoretical curves have not been fitted to any parameters, other than a scale factor of $16/3\sqrt{3}$ to normalize the curve in Fig. 6(b).

IV. DISCUSSION

In the previous sections we have demonstrated a chiral optical response arising from interference effects associated with surface plasmons. The results of simulations and experiments are consistent with our analytical model of LSP resonances. On this basis we propose that the failure of the planar chiral structures in Figs. 1(a)–1(c) to respond to optical chirality is due to a combination of two effects: (1) LSP modes with orthogonal dipole moments and (2) degenerate modes resulting in zero phase differences. For example, the symmetry of the structures in Figs. 1(a) and 1(c) is such that there will be two degenerate modes with orthogonal dipole moments, so there will be no contribution to the chiral optical response from interference effects. The structure in Fig. 1(b) is less symmetric but is likely to have two nondegenerate but orthogonal modes. We have performed simulations similar to those discussed by Davis *et al.*[18] which confirm this, but the result depends to some degree on the aspect ratio of the structure. In all cases, these effects are consequences of the geometric symmetry of the nanostructures which is broken for the structures in Figs. 1(d)–1(f). The asymmetry is important to prevent the resonant modes from being geometrically orthogonal and degenerate.

The extinction difference associated with LCP and RCP, as measured in our optical experiments, has the appearance of a large circular dichroism. However there are significant differences. Inverting the sample so that light is incident from the opposite direction also inverts the chiral optical response. The analytical model predicts this sign reversal. Referring to Eq. (4), a change in the direction of the incident light, so that $-\hat{z} \rightarrow +\hat{z}$, is equivalent to inverting all the structures (or inverting the sample) such that $\theta_r^k \rightarrow \pi - \theta_r^k$ whereby $\sin(\theta_r^k - \theta_r^j) \rightarrow -\sin(\theta_r^k - \theta_r^j)$. The sign change inverts the chiral response. This effect has been observed previously, both in the microwave region[25,26] and in the near-infrared region.[15] It is important to note that optically active materials do not have this property.[15]

When viewed away from the surface normal, the interference effect also creates a chiral optical response for orthogonal but nondegenerate LSP modes. This is evident in Eq. (3). For example, a thin planar structure with no dipole moment normal to the surface such that $p_z^j = 0$ has $N_r^{kj} = -\sin^2\xi\cos(\theta_r^k - \psi)\cos(\theta_r^j - \psi)/2$. When the LSP modes have orthogonal dipole moments then $\sin 2(\theta_r^k - \theta_r^j) = 0$ but $N_r^{kj}\sin(\theta_r^k - \theta_r^j) \neq 0$ for $\xi > 0$. This leads to a dependence of the scattered power in Eq. (4) on the chirality of the incident light. The intensity of the scattered field also appears as CD but is again an interference effect. Similar effects are observed in subwavelength arrays of holes[27] which are attributed to spatial dispersion.

As we have discussed, the interference effect associated with the chiral optical response differs from optical activity and circular dichroism. It is also quite different from interference associated with diffraction from periodic structures, since it can occur with structures that are significantly smaller than the wavelength of light. Furthermore it differs from interference effects associated with propagation phase shifts, as might result from double-slit interference. There is no dependence of the chiral optical response in Eq. (4) that depends on the propagation distance to the point of observation or on the separation between the nanostructures. The interference effect we have described is uniquely related to phase shifts associated with the resonances of the metal structures and to phase shifts associated with the rotation of the electric field vector. This does not imply that all chiral optical effects associated with plasmonic structures can be attributed to this interference effect only. Under the appropriate symmetry conditions true optical activity and circular dichroism can arise that are not accounted for in our model.

V. CONCLUSION

We have studied the chiral optical response from subwavelength arrays of metal structures supporting localized surface plasmon resonances. We have demonstrated that a strong dependence on the chirality of the incident light can arise from an interference effect associated with phase shifts in the surface plasmon modes. An analytical model based on the electrostatic approximation was used to determine the key factors that affect the response. The predictions of the model were verified using

both numerical simulations and experiments on metamaterials created from subwavelength arrays of gold rods on a glass substrate. We showed that it is necessary to have at least two nondegenerate resonant modes and that their dipole moments must not be parallel or perpendicular. The chiral response is related to phase differences in the radiation emitted from the surface plasmons and differs from the response of optically active materials and other interference effects. Our method provides criteria for designing new plasmonic nanostructures with strong chiral optical response.

ACKNOWLEDGMENTS

The authors wish to thank Harald Giessen and colleagues for their helpful comments and Matteo Altissimo for providing assistance in the nanofabrication process.

[1] Y. Tang and A. E. Cohen, Phys. Rev. Lett. **104**, 163901 (2010).
[2] Y. Tang and A. Cohen, Science **332**, 333 (2011).
[3] B. Canfield, S. Kujala, M. Kauranen, K. Jefimovs, T. Vallius, and J. Turunen, Appl. Phys. Lett. **86**, 183109 (2005).
[4] B. Canfield, S. Kujala, K. Laiho, K. Jefimovs, J. Turunen, and M. Kauranen, Opt. Express **14**, 950 (2006).
[5] A. V. Rogacheva, V. A. Fedotov, A. S. Schwanecke, and N. I. Zheludev, Phys. Rev. Lett. **97**, 177401 (2006).
[6] M. Decker, M. W. Klein, M. Wegener, and S. Linden, Opt. Lett. **32**, 856 (2007).
[7] E. Plum, V. A. Fedotov, A. S. Schwanecke, N. I. Zheludev, and Y. Chen, Appl. Phys. Lett. **90**, 223113 (2007).
[8] H. Husu, B. K. Canfield, J. Laukkanen, B. Bai, M. Kuittinen, J. Turunen, and M. Kauranen, Appl. Phys. Lett. **93**, 183115 (2008).
[9] D.-H. Kwon, P. L. Werner, and D. H. Werner, Opt. Express **16**, 11802 (2008).
[10] V. K. Valev, N. Smisdom, A. V. Silhanek, B. De Clercq, W. Gillijns, M. Ameloot, V. V. Moshchalkov, and T. Verbiest, Nano Lett. **9**, 3945 (2009).
[11] M. Decker, R. Zhao, C. Soukoulis, S. Linden, and M. Wegener, Opt. Lett. **35**, 1593 (2010).
[12] E. Hendry, T. Carpy, J. Johnston, M. Popland, R. V. Mikhaylovskiy, A. J. Lapthorn, S. M. Kelly, L. D. Barron, N. Gadegaard, and M. Kadodwala, Nature Nanotechnol. **5**, 783 (2010).
[13] D. N. Chigrin, C. Kremers, and S. V. Zhukovsky, Appl. Phys. B **105**, 81 (2011).
[14] S. V. Zhukovsky, C. Kremers, and D. N. Chigrin, Opt. Lett. **36**, 2278 (2011).
[15] M. Hentschel, M. Schäferling, T. Weiss, N. Liu, and H. Giessen, Nano Lett. **12**, 2542 (2012).
[16] T. J. Davis, K. C. Vernon, and D. E. Gómez, Phys. Rev. B **79**, 155423 (2009).
[17] T. J. Davis, D. E. Gómez, and K. C. Vernon, Phys. Rev. B **81**, 045432 (2010).
[18] T. J. Davis, D. E. Gómez, and K. C. Vernon, Nano Lett. **10**, 2618 (2010).
[19] T. J. Davis, D. E. Gómez, and K. C. Vernon, Phys. Rev. B **82**, 205434 (2010).
[20] T. Davis, M. Hentschel, N. Liu, and H. Giessen, ACS Nano **6**, 1291 (2012).
[21] T. Davis, K. Vernon, and D. Gómez, Opt. Express **17**, 23655 (2009).
[22] E. Prodan, C. Radloff, N. Halas, and P. Nordlander, Science **302**, 419 (2003).
[23] D. E. Gómez, K. C. Vernon, and T. J. Davis, Phys. Rev. B **81**, 075414 (2010).
[24] J. D. Jackson, *Classical electrodynamics*, 2nd ed. (John Wiley & Sons Inc, New York, 1975).
[25] V. A. Fedotov, P. L. Mladyonov, S. L. Prosvirnin, A. V. Rogacheva, Y. Chen, and N. I. Zheludev, Phys. Rev. Lett. **97**, 167401 (2006).
[26] E. Plum, V. Fedotov, and N. Zheludev, Appl. Phys. Lett. **94**, 131901 (2009).
[27] B. Gompf, J. Braun, T. Weiss, H. Giessen, M. Dressel, and U. Hübner, Phys. Rev. Lett. **106**, 185501 (2011).